

Particle production in the toy world: multiplicity distribution and entropy

Eugene Levin^{1,*}

¹*Department of Particle Physics, Tel Aviv University, Tel Aviv 69978, Israel*

(Dated: December 4, 2024)

In this paper we found the multiplicity distribution of the produced dipoles in the final state for dipole-dipole scattering in the zero dimension toy models. This distribution shows the great differences from the distributions of partons in the wave function of the projectile. However, in spite of this difference the entropy of the produced dipoles turns out to be the same as the entropy of the dipoles in the wave function. This fact is not surprising since in the parton approach only dipoles in the hadron wave function which can be produced at $t = +\infty$ and measured by the detectors. We can also confirm the result of Kharzeev and Levin that this entropy is equal to $S_E = \ln(xG(x))$, where we denote by xG the mean multiplicity of the dipoles in the deep inelastic scattering. The evolution equations for σ_n are derived.

PACS numbers: 13.60.Hb, 12.38.Cy

Contents

I. Introduction	1
II. Scattering amplitudes in zero transverse dimensions models	3
III. AGK cutting rules and multiparticle production in the UTM	5
A. Continuous approximation	5
B. Arbitrary Y	7
C. Interaction with nuclei	9
IV. Evolution of σ_n in parton approach	9
A. BFKL cascade	10
B. UTM cascade	10
1. Elastic amplitude	11
2. Single diffraction	12
3. σ_1	13
4. σ_n	13
V. Entropy of produced particles	14
A. Continuous approximation	14
B. Arbitrary Y	15
VI. Conclusions	16
A. Distribution of the produced gluons in the BFKL Pomeron	16
B. The Pomeron calculus of the UTM	17
1. The first Pomeron diagrams	18
2. Summing enhanced diagrams	19
3. Multiplicity distribution for the 'dressed' Pomeron	20
References	21

I. INTRODUCTION

Zero transverse dimension toy models can be viewed as a realization of the Pomeron calculus or more generally of Reggeon Field Theory (RFT). Over the years they have been intensively used to model high energy collisions in QCD. These models[1–17] encode various fundamental features of QCD such as unitarity, but are much simpler than

the latter and frequently solvable analytically. Hence they provide a valuable playground to gain intuition about the dynamics of real QCD.

In this paper, we continue the exploration of the toy world following our early papers on the subject, Ref. [15–17]. We consider dipole-dipole scattering and focus on particle production in the final state. There are two motivations behind this work. First, multiplicity distribution of produced particles is an important experimental observable measured in most of the experiments ranging from DIS to heavy ion collisions¹[18–50]. Particularly, measuring the multiplicity distribution of soft hadrons in heavy ion collisions was instrumental to identify thermalization and hydrodynamization of produced QGP. A quantity tightly related to the multiplicity distribution is the entropy of produced particles. It is believed to provide a valuable insight about particle production mechanism, particularly about the decoherence processes taking place throughout the scattering process. There are quite a few theoretical approaches to entropy production in high energy collisions [51–72], which we will not review here. Experimental works on the subject have been reported too [18].

As the second motivation behind this work, we were triggered by the recent ideas put forward in [70–72]. There, the $2 \rightarrow n$ process has been identified with formation of a maximal entropy classical state, the *saturnon*. Furthermore, this classical state was speculated to mimic a black hole formation through two graviton collision. One of the key assumptions of [70–72] is about the large n behavior of the $2 \rightarrow n$ cross section, $\sigma(2 \rightarrow n)$.

Having a realistic toy model of particle production at hand makes it possible to check the main assumption of these papers.

Our discussion starts (Section 2) from reviewing two toy models. The first one is the BFKL cascade model which mimics the Mueller’s dipole model in QCD [73]. This model lacks both s and t -channel unitarity [15, 74] and hence has to be corrected. A more realistic model is the Unitary Toy Model (UTM) first introduced in [7] and later explored in [12, 15, 16, 74]. These past studies have been mainly focused on formulation of RFT and computation of total S -matrix.

Particle production in the toy world was originally addressed by Mueller and Salam in [7]. Using the AGK cutting rules [75] applied to the BFKL cascade model, they derived a formula (denoted as MS formula below) for multiplicity distribution of produced particles (dipoles). The MS formula turns out to be frame dependent (violates the t -channel unitarity) and hence requires revision. Our prime goal in this paper is precisely to fill this gap. We believe that all defects of the MS formula stem from the violation of t -channel unitarity in the BFKL cascade model. Hence, we are going to discuss mainly the UTM which is free from these shortcomings. While the total S -matrix is based on the knowledge of elastic amplitudes only, particle production requires additional information about inelastic processes. Our basic ideas are the same as in Ref.[7]: we are going to explore the fact that the scattering amplitudes in all known zero dimension models can be calculated in the Pomeron calculus. First, we recall that it is proven in Refs.[81, 82] that the s -channel unitarity for the BFKL Pomeron has the form:

$$2 \operatorname{Im} G_{\mathcal{P}}(Y) \equiv 2 N(Y) = \sigma_{in}^{\text{BFKL}}(Y) \quad (1)$$

where $G_{\mathcal{P}}$ is the Green’s function for the BFKL Pomeron and $\sigma_{in}^{\text{BFKL}}(Y)$ is the inelastic cross sections of produced gluons with mean multiplicity $\bar{n} = \Delta Y$, where Δ is the intercept of the BFKL Pomeron. We also know that produced gluons have the Poisson distribution with this mean multiplicity (see Ref.[82] and appendix A).

The second ingredient is the AGK cutting rules[75], which allow us to calculate the imaginary part of the scattering amplitude, that determines the cross sections, through the powers of $\operatorname{Im} G^{\text{BFKL}}(Y)$. Our master formula takes the form of convolution for the cross section of produced n gluons:

$$\sigma_n(Y) = \sum_k \underbrace{\sigma_k^{\text{AGK}}(Y)}_{\propto (\operatorname{Im} G_{\mathcal{P}})^k} \underbrace{\frac{(\Delta k Y)^n}{n!} e^{-\Delta k Y}}_{\text{Poisson distribution}} \xrightarrow{Y \gg 1} \sigma_{k=n/(\Delta Y)}^{\text{AGK}}(Y) \quad (2)$$

A mindful reader recognized that our approach has been very successful in describing the multiparticle production processes in the framework of soft Pomeron calculus (see Ref.[83]) and follows the main ideas of Ref.[7]. This approach has at least two advantages: (i) it can be easily generalized to the QCD case; and (ii) it replaces in economic way a mess of parton interactions during propagation of the parton cascade (see Fig. 1) from the moment of interaction of wee parton with the target ($t = 0$ in Fig. 1) till it reaches the detectors ($t = \infty$ in Fig. 1).

¹ It is almost impossible to collect all references on the measurement of multiplicity. We concentrated mostly on high energy pp collisions since in the paper we consider this particular process.

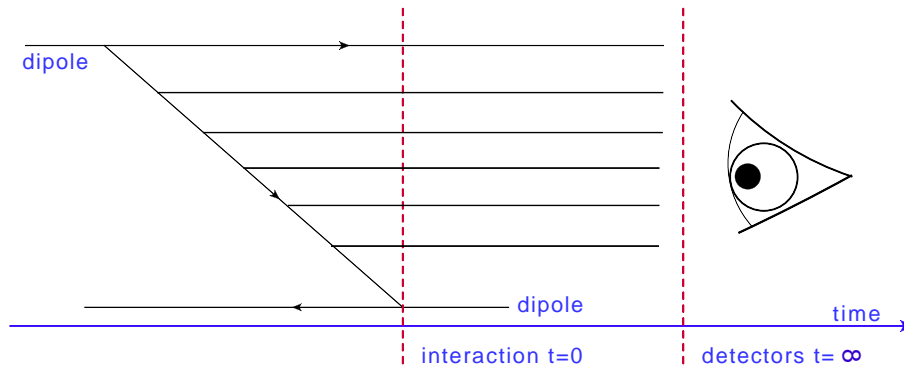


FIG. 1: The sketch of dipole-dipole interaction in the parton approach. The lines denote partons (dipoles),

In section II we mostly review the results of Refs.[15–17]. The section III, IV and V are the main part of our paper in which discuss our approaches to production of dipoles. In section III we compute the dipole multiplicity distributions in the final state based of the AGK cutting rules and the structure of the Pomeron exchange (see Eq. (1) and Eq. (2)). This distributions show quite different behaviour in comparison with the multiplicity distribution in the wave function of the projectile.

In section IV we generalize the approach of Refs.[14, 77–80] to the UTM cascade and show that the AGK cutting rules can be replaced by the evolution equations for σ_n .

In section V we find that the entropy of the produced gluons turns out to be the same at the entropy of the dipoles in the wave partonic function of the projectile. In conclusions we summarize our results.

II. SCATTERING AMPLITUDES IN ZERO TRANSVERSE DIMENSIONS MODELS

Pomeron calculus in zero transverse dimensions models QCD for dipoles of fixed sizes. Due to simplicity of the toy models of this type, they can be formulated as Reggeon Field Theory (RFT) for interacting bare Pomerons, and studied analytically. By bare Pomeron we mean a BFKL-like elastic scattering amplitude for dipole-dipole scattering (below, we will also refer to "cut" Pomerons, which is a total inelastic cross section in the same dipole-dipole process). One hopes that the study of these models is a useful endeavor assuming they retain some important features of real QCD.

Several models of this type have been recently considered in the literature. They all share the following simple probabilistic expression for the total S -matrix for scattering of n dipoles of the projectile on m dipoles of the target

$$S(Y) = \sum_{n,m} e^{-m n \gamma} P_n^P(Y_0) P_m^T(Y - Y_0) \quad (3)$$

Here $\gamma \sim \alpha_s^2$ is the Born approximation to the dipole-dipole scattering amplitude at energies. $P_n^P(Y_0)$ is the probability to find n dipoles in the projectile boosted to rapidity Y_0 , and similarly for the target. The probabilities are found by solving the evolution equation in rapidity, and it is in the form of this equation that the models differ from each other. The important consistency condition on the evolution is t -channel unitarity, which is essentially the requirement that the S -matrix does not depend on the reference frame, that is the choice of Y_0 at a fixed Y [7, 12, 15–17].

In this section we discuss the scattering amplitude for the unitarity toy model (UTM). This model satisfies both the t (see Refs.[7, 12, 15] and s (see Ref.[15]) channel unitarity conditions. Requiring Y_0 independence of the S -matrix in Eq. (3) one is lead to the evolution equation for $P_n^{\text{UTM}}(Y)$ [7, 12]:

$$\frac{dP_n^{\text{UTM}}(Y)}{dY} = -\frac{\Delta}{1-e^{-\gamma}} (1 - e^{-\gamma n}) P_n^{\text{UTM}}(Y) + \frac{\Delta}{1-e^{-\gamma}} (1 - e^{-\gamma(n-1)}) P_{n-1}^{\text{UTM}}(Y) \quad (4)$$

Eq. (4) can be rewritten as the general equation for the generating function of UTM:

$$\frac{\partial}{\partial \tilde{Y}} Z(u, \tilde{Y}) = -(1-u) \left(1 - e^{-\gamma u \frac{\partial}{\partial u}}\right) Z(u \tilde{Y}) = (u-1) \left(Z(u, \tilde{Y}) - Z(e^{-\gamma} u, \tilde{Y}) \right) \quad (5)$$

where[17]

$$Z(u, \tilde{Y}) = \sum_{n=0}^{\infty} C_n(\gamma) \Phi_n(u, \gamma) e^{\Delta_n \tilde{Y}} \quad (6)$$

$\Phi_n(u, \gamma)$ are the eigenfunctions of the hamiltonian: $\mathcal{H} = -(1-u) \left(1 - e^{-\gamma u \frac{\partial}{\partial u}}\right)$ with the eigenvalues $\Delta_n = \exp(n\gamma) - 1$. $C_n(\gamma) = \exp\left(\frac{n(n+1)}{2}\gamma\right)$. The scattering amplitude for dipole-dipole scattering takes the form[17]:

$$S(\tilde{Y}) = Z(e^{-\gamma}, \tilde{Y}) = \sum_{n=0}^{\infty} C_n(\gamma) \Phi_n(e^{-\gamma}, \gamma) e^{\Delta_n \tilde{Y}} \quad (7)$$

where we use Eq. (6). For small γ $C_n \Phi_n(1 - \gamma, \gamma) = (-\gamma)^n n! + O(\gamma^{n+1})$, leading to

$$S(\tilde{Y}) = \sum_{n=0}^{\infty} (-\gamma)^n n! e^{\Delta_n \tilde{Y}} \left\{ 1 + O(\gamma) \right\} \quad (8)$$

Eq. (8) has natural interpretation in the Pomeron calculus (see appendix B and Fig. 10).

Using $n! = \int_0^{\infty} d\tau e^{-\tau} \tau^n$ we can rewrite Eq. (8) as follows:

$$S(\tilde{Y}) = \int_0^{\infty} d\tau e^{-\tau} \sum_{n=0}^{\infty} (-\gamma \tau)^n e^{\Delta_n \tilde{Y}} \quad (9)$$

Eq. (8) and Eq. (9) give the asymptotic series for the scattering amplitude. However, one can see that each term of this series has intercept which is large that $\gamma n(\Delta_n = e^{\gamma n} - 1 > \gamma n)$ and therefore, series of Eq. (9) cannot be Borel summed. In Ref.[17] it is suggested the following expansion for summing these series

$$\exp(\Delta_n \tilde{Y}) = e^{-\tilde{Y}} \sum_{j=0}^{\infty} \frac{e^{\gamma n j} \tilde{Y}^j}{j!}. \quad (10)$$

Plugging Eq. (10) into Eq. (9) we obtain

$$S(\tilde{Y}) = \int_0^{\infty} d\tau e^{-\tau} \sum_{n=0}^{\infty} (-\gamma \tau)^n e^{-\tilde{Y}} \sum_{j=0}^{\infty} \frac{e^{\gamma n j} \tilde{Y}^j}{j!} \quad (11)$$

Both series are absolutely converged and changing the order of summation we have

$$S(\tilde{Y}) = e^{-\tilde{Y}} \sum_{j=0}^{\infty} \frac{\tilde{Y}^j}{j!} \int_0^{\infty} d\tau e^{-\tau} \sum_{n=0}^{\infty} (-\gamma \tau)^n e^{\gamma n j} \quad (12)$$

Summing over n we obtain

$$S(\tilde{Y}) = e^{-\tilde{Y}} \sum_{j=0}^{\infty} \frac{\tilde{Y}^j}{j!} \int_0^{\infty} d\tau e^{-\tau} \frac{1}{1 + \tau \gamma N_j} = e^{-\tilde{Y}} \sum_{j=0}^{\infty} \frac{\tilde{Y}^j}{j!} \frac{1}{\gamma N_j} \exp\left(\frac{1}{\gamma N_j}\right) \Gamma\left(0, \frac{1}{\gamma N_j}\right) \quad (13)$$

where $N_j = e^{\gamma j}$. It is easy to see that the series in Eq. (13) is absolutely converged and give the analytical function for the scattering amplitude. It is worthwhile mentioning that Eq. (10) and Eq. (13) give a way of summing the asymptotic series, which is quite different from the Borel summation, which is used to sum such series.

In Refs.[15, 17] it was suggested a continuous approach to the UTM in which $P_n - P_{n-1}$ were replaced by dP_n/dn and a contribution of d^2P_n/dn^2 was neglected. In this approach Eq. (9) takes the form:

$$\begin{aligned} S^{CA}(\tilde{Y}) &= \int_0^{\infty} d\tau e^{-\tau} \sum_{n=0}^{\infty} (-\gamma \tau)^n e^{\Delta_n \tilde{Y}} = \int_0^{\infty} d\tau e^{-\tau} \frac{1}{1 + \gamma \tau e^{\Delta \tilde{Y}}} \\ &= \frac{1}{\gamma N(\tilde{Y})} \exp\left(\frac{1}{\gamma N(\tilde{Y})}\right) \Gamma\left(0, \frac{1}{\gamma N(\tilde{Y})}\right) \end{aligned} \quad (14)$$

where $N(\tilde{Y}) = e^{\Delta \tilde{Y}}$ and $\Gamma(0, z)$ is incomplete Gamma function. It is worthwhile mentioning that in Eq. (14) the Borel summation has been used. It is shown in Ref.[17] that Eq. (14) can be reproduced directly from Eq. (3) in the BFKL limit where in Eq. (4) we replace $e^{\gamma n}$ by $1 + \gamma n$.

The scattering with the nuclear target has been discussed in Refs. [16, 17]. From Eq. (7) this amplitude has the following form:

$$S^A(\tilde{Y}) = Z(e^{-\gamma A}, \tilde{Y}) = \sum_{n=0}^{\infty} C_n(\gamma) \Phi_n(e^{-\gamma A}, \gamma) e^{\Delta_n \tilde{Y}} \quad (15)$$

In the kinematic region $\gamma A \gtrsim 1$ but $\gamma \ll 1$ $C_n(\gamma) \rightarrow 1$ and $\Phi_n(e^{-\gamma A}, \gamma) \rightarrow (-e^{\gamma A})^n$ leading to

$$S^A(\tilde{Y}) = \sum_{n=0}^{\infty} (-e^{\gamma A})^n e^{\Delta_n \tilde{Y}} = e^{-\tilde{Y}} \sum_{j=0}^{\infty} \frac{\tilde{Y}^j}{j!} \sum_{n=0}^{\infty} (-e^{\gamma(j+A)})^n = e^{-\tilde{Y}} \sum_{j=0}^{\infty} \frac{\tilde{Y}^j}{j!} \frac{1}{1 + e^{\gamma(j+A)}} \quad (16)$$

in Eq. (15) we assume that nucleus is the state of A dipoles .

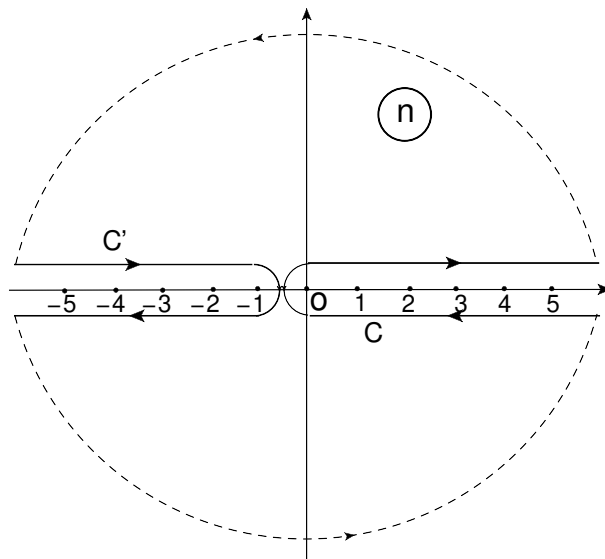


FIG. 2: The contours of integrations in complex n plane.

III. AGK CUTTING RULES AND MULTIPARTICLE PRODUCTION IN THE UTM

The scattering amplitude depends on the parton wave function of the fast projectile and on P_n (see Eq. (3)) at $\tau = 0$ in Fig. 1. Interaction of wee parton at $\tau = 0$ destroys the coherence of partons in the wave function. Hence after this interaction the partons start to interact between themselves, these interactions are difficult to tackle. In the introduction we have described our approach which is based on the AGK cutting rules and on the proven fact that imaginary part of the Pomeron Green's function leads to the cross section of the produced gluons in QCD².

A. Continuous approximation

For arbitrary Y we have to use the scattering amplitude in a general form of Eq. (7) and Eq. (13), However, in the continuous approximation we can restrict ourselves by Eq. (14) which is much simpler. It has has the following

² It should be mentioned that on QCD the partons at $\tau = 0$ are colourless dipoles while at $\tau = \infty$ the gluons are produced.

simple form

$$S(Y) = \sum_{k=0}^{\infty} (-1)^k C_k(\gamma) [N(Y)]^k; \quad C_0 = 1 \quad (17)$$

with $C_k = \gamma^k k!$. $N(Y)$ denotes the imaginary part of the Pomeron Green's function (see Eq. (1)) and it equals to $\exp(\Delta_1 \tilde{Y})$. In the toy world, as well as in QCD [73] the imaginary part of the Pomeron Green's function coincides with the multiplicity of dipoles in the BFKL cascade.

Each term in Eq. (17) is a contribution of k BFKL Pomerons. The Pomeron Green's function $G_P(Y)$ depend on rapidity but not on γ , while the dependence on γ comes through the coefficients C_k . The latter have interpretation of multi-Pomeron residues (impact factors). The expansion (Eq. (17)) is not general, because not every function $S(Y)$ is expandable in powers of $N(Y) = \text{Im}G_P(Y)$. A compact representation of Eq. (17) in the UTM has the form (see Eq. (14))

$$S^{CA} = \int_0^{\infty} dt e^{-t} \frac{1}{1 + t\gamma N(Y)} \quad (18)$$

The Pomeron plays two fold role in the scattering amplitude. First, it gives the scattering amplitude of two dipoles at high energy. The interaction of the Pomerons with the colliding dipoles and between them provides the shadowing in the amplitude which has been taken into account in Eq. (18). Second, the imaginary part of the Pomeron exchange due to the unitarity constraints of Eq. (1) give the cross section of produced gluons. The AGK cutting rules allows us to calculate the cross section proportional to $(\text{Im}G_P(Y))^n = (\sigma_{in}^{\text{BFKL}}(Y))^n$ ³ out of the contribution to the total cross sections of k exchanged Pomerons ($\propto G_P^k(Y)$). The AGK rules give:

$$n \geq 1: \quad \sigma_n^k(Y) = C_k (-2)^{k-n} \frac{k!}{(k-n)! n!} (\sigma_{in}^{\text{BFKL}}(Y))^n \quad (19a)$$

$$n = 0: \quad \sigma_0^k(Y) = \left(2 - 2^k\right) C_k \left(-N(Y)\right)^k; \quad (19b)$$

Here $n = 0$ is the diffractive dissociation.

The total "production" of n cut Pomerons is the sum over all exchanges ($k \geq n$):

$$\begin{aligned} \sigma_n^{\text{AGK}} &= \sum_{k=n}^{\infty} \sigma_n^k = \sum_{k=n}^{\infty} C_k (-2)^{k-n} \frac{k!}{(k-n)! n!} (\sigma_{in}^{\text{BFKL}}(Y))^n \\ &= \sum_{k=n}^{\infty} (-1)^{k-n} C_k (2N(Y))^k \frac{k!}{(k-n)! n!} \end{aligned} \quad (20)$$

where Eq. (1) was used to get the last expression.

While for the UTM model, the coefficients C_k are known explicitly, in general they could also be conveniently expressed as follows:

$$C_k = \frac{(-1)^k}{k!} \frac{d^k}{dN^k} S(Y)|_{N=0} \quad (21)$$

Substituting C_k into Eq. (20),

$$\sigma_n^{\text{AGK}}(Y) = \int_0^{\infty} dt e^{-t} \frac{(2t\gamma N(Y))^n}{(1 + 2t\gamma N(Y))^{n+1}} = \frac{1}{2\gamma N(Y)} k! U\left(k+1, 1, \frac{1}{2\gamma N(Y)}\right) \quad (22)$$

³ This contribution in the widely accepted slang is called the contribution of k cut Pomerons.

$U(a,b,z)$ is the Tricomi confluent hypergeometric function (see Ref.[76], formula **13.1.3**). We note two interesting limits of Eq. (22):

$$\sigma_k(Y < Y_{max}) = \frac{1}{2\gamma N} k! U\left(k+1, 1, \frac{1}{2\gamma N}\right) \rightarrow \begin{cases} \frac{1}{\gamma N} K_0\left(2\sqrt{\frac{k+1}{2\gamma N}}\right) & \text{for } 2\gamma N k > 1; \\ k!(2\gamma N)^k & \text{for } 2\gamma N k < 1; \end{cases} \quad (23)$$

Coming back to Eq. (23) one can see that we indeed have $\sigma(2 \rightarrow n)$, which behaves as $\sigma(2 \rightarrow n) = C_n n! \alpha^n$ [71, 72] where α is the four boson coupling constant is small in the t'Hooft limit: $\alpha \rightarrow 0, \lambda_t = \alpha N_c = \text{finite}$. However, α in Eq. (23) is replaced by the BFKL contribution: $2\gamma N(Y)$. Note that this contribution gives the scattering amplitude of two dipoles (four dipoles interaction) but depends on energy increasing with it. Due to this growth, at large energies $\sigma_n \sim n!(2\gamma N)^n$ does not contribute (see Eq. (23)) and the unitarity is saturated by the states with multiplicities $n \geq N$. None of these states look classical.

Summing over n (the sum starts from $n = 1$) we obtain the total inelastic cross section

$$\sigma_{in} = \sum_{n=1}^{\infty} \sigma_n^{AGK} = 1 - S(Y)|_{N \rightarrow 2N} \quad (24)$$

In the BFKL formalism (see appendix A), the inelastic cross section for production of n - partons ($\sigma_n^{\text{BFKL}}(Y)$) from a single Pomeron obeys the evolution equation

$$\frac{d\sigma_n^{\text{BFKL}}(Y)}{dY} = \Delta \sigma_{n-1}^{\text{BFKL}}(Y) \quad (25)$$

The solution takes the form:

$$\sigma_n^{\text{BFKL}}(Y) = 2 \frac{(\Delta Y)^n}{n!}; \quad \sigma_{in}^{\text{BFKL}} = \sum_{n=0}^{\infty} \sigma_n^{\text{BFKL}}(Y) = 2 \exp(\Delta Y) = 2N \quad (26)$$

consistently with the unitarity condition of Eq. (1). Here the factor 2 comes from the unitarity condition for $n = 0$. The probability $\mathcal{P}_n^{\text{P}}(Y)$ to find n partons in the final state is thus

$$\mathcal{P}_n^{\text{P}}(Y) = \frac{\sigma_n^{\text{BFKL}}(Y)}{\sum_{n=0}^{\infty} \sigma_n^{\text{BFKL}}(Y)} = \frac{(\Delta Y)^n}{n!} e^{-\Delta Y} \quad (27)$$

which is a Poisson distribution with the average number of partons $\bar{n}_1 = \Delta Y = \ln N$. This is the result for a single cut Pomeron. For k cut Pomerons, the distribution is Poisson again, but now with the average number $\bar{n}_k = k \bar{n}_1 = k \Delta Y = \ln N^k$. This corresponds to probabilities $\mathcal{P}_n^{\text{P}}(kY)$.

To find the multiplicity distribution of particles in the final states one needs to convolute $\sigma_k(Y)$ from (22) with the distribution of particles inside k cut Pomerons Eq. (27):

$$\sigma_n^{f.s.}(Y) = \sum_{k=1}^{\infty} \sigma_k^{AGK}(Y) \mathcal{P}_n^{\text{P}}(kY) \quad (28)$$

In Eq. (28) f.s. stands for the final state.

B. Arbitrary Y

For general approach we have to use the scattering amplitude in a general form of Eq. (7) and Eq. (13).

The AGK cutting rules [75] allows us to calculate the contributions of n -cut Pomerons if we know F_k : the contribution of the exchange of k -Pomerons to the cross section. They take the form:

$$n \geq 1 : \sigma_n^k(Y) = (-1)^{k-n} \frac{k!}{(n-k)! n!} 2^k F_k(\gamma, Y) \quad (29a)$$

$$n = 0 : \sigma_0^k(Y) = (-1)^k \left(2^k - 2 \right) F_k(\gamma, Y); \quad (29b)$$

$$\sigma_{tot} = 2 \sum_{k=1}^{\infty} (-1)^{k+1} F_k(\gamma, Y); \quad (29c)$$

where σ_{tot} is the total cross section and σ_0 denotes the cross section with the multiplicity of produced dipoles which is much less than ΔY . In other words, it is the cross section of the diffraction production. From Eq. (9) one can see that

$$F_k(\gamma, Y) = \int_0^{\infty} d\tau e^{-\tau} (\tau \gamma)^k e^{\Delta_k \tilde{Y}} \quad (30)$$

Using Eq. (10) we can rewrite Eq. (30) in the following form

$$F_k(\gamma, Y) = e^{-\tilde{Y}} \sum_{j=0}^{\infty} \frac{e^{\gamma k j} \tilde{Y}^j}{j!} \int_0^{\infty} d\tau e^{-\tau} (\tau \gamma)^k \quad (31)$$

Bearing in mind Eq. (29a) we can introduced

$$\sigma_n^{\text{AGK}} = \sum_{k=n}^{\infty} (-1)^{k-n} \frac{k!}{(k-n)! n!} 2^k F_k(\gamma, Y); \quad \sigma_{in}^{\text{AGK}} = \sum_{n=1}^{\infty} \sigma_n^{\text{AGK}} \quad (32)$$

which is the cross section of production of n -cut Pomerons in our process and σ_{in}^{AGK} is the inelastic cross section.

Plugging Eq. (30) into Eq. (32) and summing over k we obtain:

$$\sigma_n^{\text{AGK}} = e^{-\tilde{Y}} \sum_{j=0}^{\infty} \frac{Y^j}{j!} \int_0^{\infty} d\tau e^{-\tau} \frac{(2\tau \gamma N_j)^n}{(1 + 2\tau \gamma N_j)^{n+1}} = e^{-\tilde{Y}} \sum_{j=0}^{\infty} \frac{\tilde{Y}^j}{j!} n! \frac{1}{\gamma N_j} U\left(n+1, 1, \frac{1}{\gamma N_j}\right) \quad (33)$$

Using Eq. (23) for $U\left(n+1, 1, \frac{1}{\gamma N_j}\right)$ we can take the integral over j in Eq. (34) using the method of steepest descent. The equation for the saddle point value of j $j = j_{SP}$ takes the form:

$$\ln \tilde{Y} - \ln j_{SP} + \gamma \sqrt{\frac{k+1}{2\gamma N_{j_{SP}}}} = 0 \quad (34)$$

The solution to Eq. (34) at large \tilde{Y} has the form:

$$j_{SP} = \tilde{Y} \exp\left(\gamma \sqrt{\frac{k+1}{2\gamma N(\tilde{Y})}}\right) \quad \text{with} \quad N(\tilde{Y}) = e^{\gamma \tilde{Y}} \quad (35)$$

Plugging Eq. (35) into Eq. (33) we obtain:

$$\sigma_n^{\text{AGK}} = \frac{1}{\gamma N(\tilde{Y})} \exp\left(-2 \sqrt{\frac{k+1}{2\gamma N(\tilde{Y})}} - \gamma^2 \tilde{Y} \frac{k+1}{2\gamma N(\tilde{Y})}\right) \quad (36)$$

In Eq. (36) we use the asymptotic expression for $K_0\left(2\sqrt{\frac{k+1}{2\gamma N(\tilde{Y})}}\right)$ for simplicity.

Fig. 3 illustrates the difference between the exact solution to Eq. (34) and the approximate solution at large \tilde{Y} .

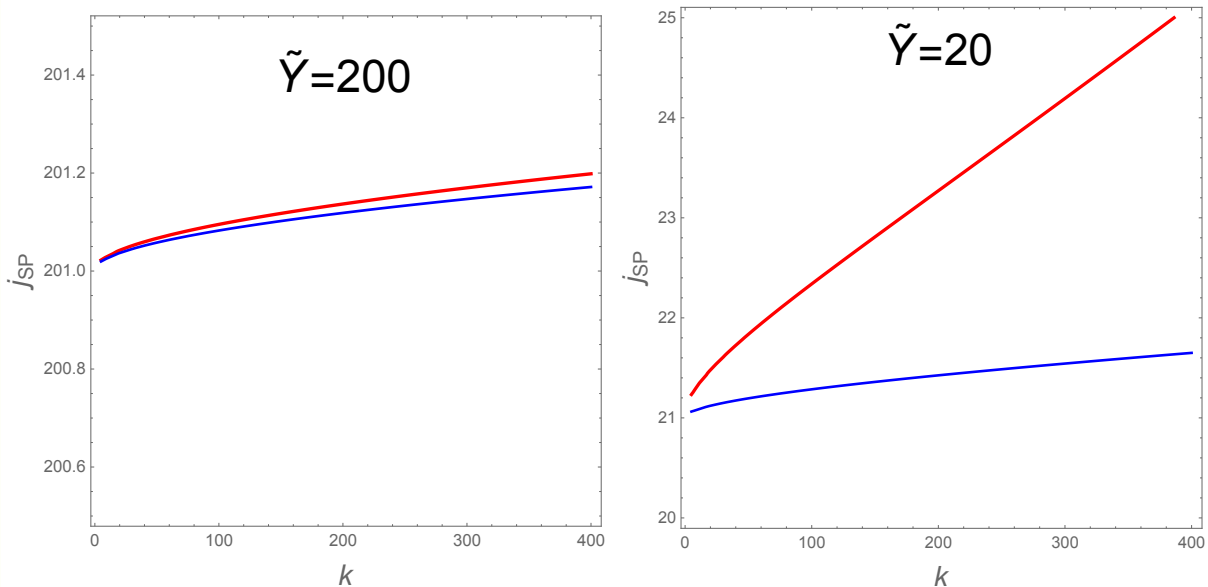


FIG. 3: j_{SP} of Eq. (34) versus n at different Y (red curves). The blue curves show the saddle point value of j_{SP} given by Eq. (35). $\Delta = 0.2$ and $\gamma = 0.025$.

C. Interaction with nuclei

The scattering matrix for interaction with a nucleus target has been written in Eq. (16). Applying the AGK cutting rules we obtain for $\sigma_n^{AGK,A}$ the following expression:

$$\begin{aligned} \sigma_n^{AGK,A} &= e^{-\tilde{Y}} \sum_{j=0}^{\infty} \frac{\tilde{Y}^j}{j!} \frac{(2\gamma e^{\gamma(j+A)})^n}{(1 + 2\gamma e^{\gamma(j+A)})^{n+1}} \\ &\xrightarrow{\gamma e^{\gamma(j+A)} \gg 1} e^{-\tilde{Y}} \sum_{j=0}^{\infty} \frac{\tilde{Y}^j}{j!} \frac{1}{2\gamma e^{\gamma(j+A)}} \exp\left(-\frac{n-1}{2\gamma e^{\gamma(j+A)}}\right) \end{aligned} \quad (37)$$

Eq. (37) differs from the BFKL multiplicity distribution due to sum over j which stems from the enhanced diagrams. Plugging in this equation $j = \tilde{Y}$ we obtain that

$$\sigma_n^{AGK,A} = \frac{1}{2\gamma e^{\gamma(j\tilde{Y}+A)}} \exp\left(-\frac{n-1}{2\gamma e^{\gamma(\tilde{Y}+A)}}\right) \quad (38)$$

which is the BFKL distribution with the mean multiplicity in $e^{\gamma A}$ times larger than that in the BFKL cascade for one dipole.

IV. EVOLUTION OF σ_n IN PARTON APPROACH

It has been shown in Refs.[77, 78] (see also Refs.[14, 80]) that instead of using the AGK cutting rules, we can write the evolution equation in parton approach. This equation is based on two principle ingredients. The first one is that only partons in the parton wave function of the fast hadron at $t \rightarrow -\infty$ in Fig. 4 can be produced at $t \rightarrow +\infty$ and are measured by our detectors. This point was proven in Refs.[77, 78] and the proof is used the results of Ref.[79]. These papers show that neither production of the new partons nor annihilation of the partons in the hadronic wave function contribute to σ_n , including single diffraction. The proof is general and does not depend on the specific interaction between partons. Actually this feature allows us to apply parton approach for discussing the multiplicity distributions

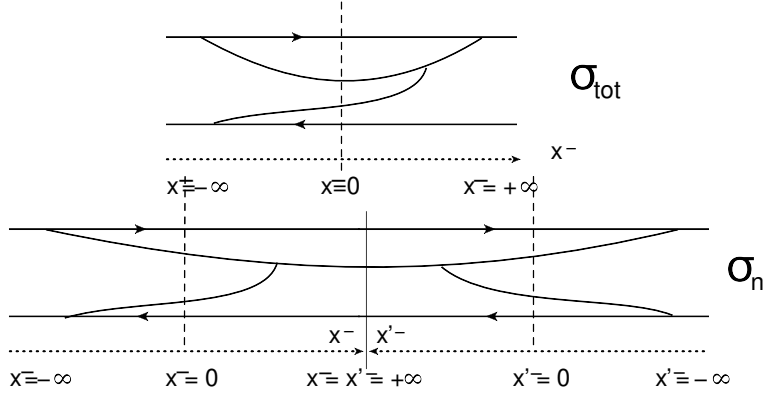


FIG. 4: A comparison of calculations of σ_{tot} and σ_n in parton approach. At $t = 0$ the parton cascade interacts with the target. At $t = +\infty$ the produced partons are measured by the detectors.

of produced partons. It has been demonstrated[14, 78, 80] that the AGK cutting rules provides these features in the framework of the parton approach.

A. BFKL cascade

The second principle feature has been proven for the BFKL parton cascade[14, 77, 78, 80] we can write the following evolution equations (see Fig. 5) which we present for simplicity for the toy models⁴:

$$\frac{dN_0(Y)}{dY} = \Delta (N_0(Y) - N_0^2(Y)); \quad (39a)$$

$$\frac{d\sigma_{sd}(Y)}{\partial Y} = \Delta (\sigma_{sd}(Y) + \sigma_{sd}^2(Y) - 4\sigma_{sd}(Y)N_0(Y) + 2N_0^2(Y)); \quad (39b)$$

$$\frac{d\sigma_1(Y)}{dY} = \Delta (\sigma_1(Y) - 2\sigma_1(Y)(2N_0(Y) - \sigma_{sd}(Y))); \quad (39c)$$

$$\frac{d\sigma_2(Y)}{dY} = \Delta (\sigma_2(Y) + 2\sigma_2(Y)\sigma_{sd} + \sigma_1^2(Y) - 4N_0(Y)\sigma_2(Y)); \quad (39d)$$

$$\frac{d\sigma_n(Y)}{dY} = \Delta \left(\sigma_n(Y) + 2\sigma_n(Y)\sigma_{sd} + \sum_{k=1}^n \sigma_{n-k}(Y)\sigma_k(Y) - 4N_0(Y)\sigma_n(Y) \right); \quad (39e)$$

where Δ is the intercept of the BFKL Pomeron, N_0 is the imaginary part of the elastic amplitude, σ_{sd} is the cross section of the single diffraction, and σ_n is the cross section of production of $n\Delta Y$ number of partons.

The graphic forms of these equations are shown in Fig. 5. It turns out that all numerical factors in this figure reproduce the AGK cutting rules. In this figure we consider that partons in our approach are dipoles of QCD with the fixed sizes. Every equation in Fig. 5 is written for the cross section of interaction of one dipole shown by two lines with the target which is presented in the figure by vertical dotted line. This dipole decays in two dipoles which interact with the target. In the figure all possible interactions are shown with trivial factors that take into account the number of possible interactions and the shadowing due to interaction of elastic amplitude (N_0) with the cross sections in the equations: this shadowing gives the sign minus.

B. UTM cascade

Our main goal to study what happens with Eq. (39a)-Eq. (39e) in the UTM cascade.

⁴ The proof for QCD is given in Refs.[78, 80].

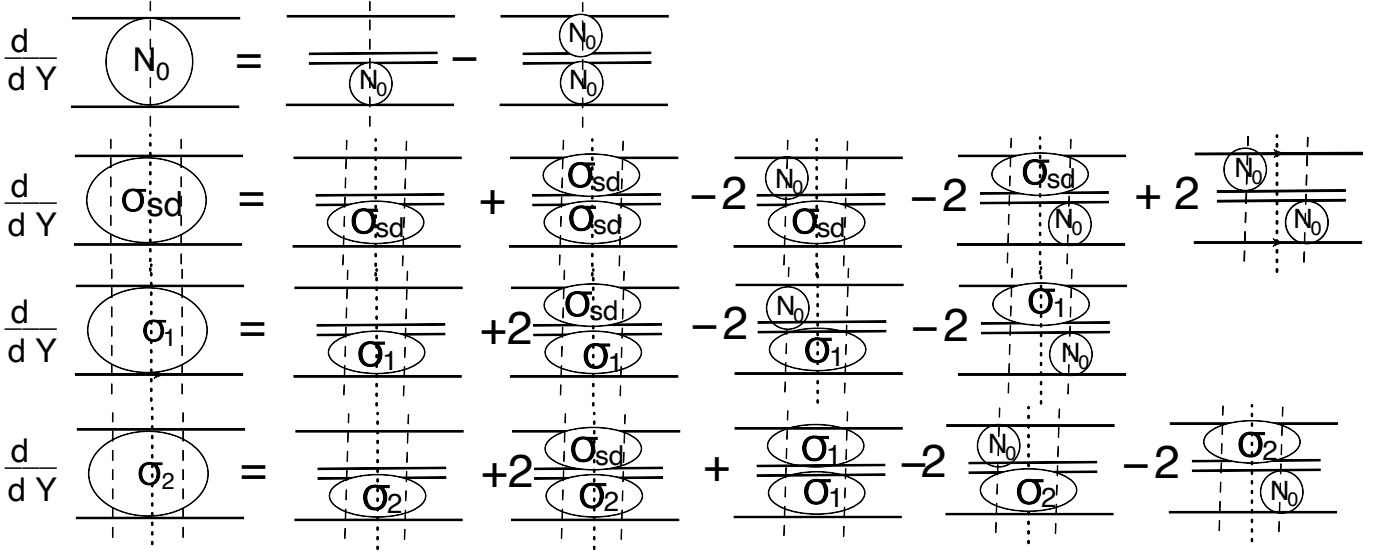


FIG. 5: The graphic form of Eq. (39a) - Eq. (39d). The vertical lines notations are the same as in Fig. 4. The Pomeron intercept is absorbed in the definition of Y .

1. Elastic amplitude

Let us start from Eq. (39a) for the elastic amplitude. We can find $\frac{dS(Y)}{dY}$ using Eq. (3) for $Y_0 = 0$ since in this model S-matrix does not depend on Y_0 . In doing so, we obtain the following equation for the scattering of two dipoles:

$$\begin{aligned} \frac{dS(Y)}{dY} &= \sum_{n=1} e^{-\gamma n} \frac{dP_n^{\text{UTM}}(Y)}{dY} = \frac{\Delta}{\gamma} (e^\gamma - 1) \sum_{n=1} \left(-e^{-\gamma n} P_n^{\text{UTM}}(Y) + e^{-2\gamma n} P_n^{\text{UTM}}(Y) \right) \\ &= \frac{\Delta}{\gamma} (e^\gamma - 1) \left(S_{d+2d}(Y) - S_{d+d}(Y) \right) \end{aligned} \quad (40)$$

where S_{d+d} is the scattering matrix of two dipoles while S_{d+2d} is the scattering matrix for interaction of one dipole with two dipoles. It is instructive to derive this formula from Eq. (8) for the scattering matrix. Indeed,

$$\frac{dS(Y)}{dY} = \sum_{n=0}^{\infty} \Delta_n C_n(\gamma) \Phi_n(e^{-\gamma}, \gamma) e^{\Delta_n \tilde{Y}} = \frac{\Delta}{\gamma} \sum_{n=0}^{\infty} (e^{\gamma n} - 1) C_n(\gamma) \Phi_n(e^{-\gamma}, \gamma) e^{\Delta_n \tilde{Y}} \quad (41)$$

In Ref.[17] we found that $C_n^{(2)}$ for the scattering amplitude with two dipoles are equal to

$$C_n^{(2)} = \frac{e^{\gamma(n+1)} - 1}{e^\gamma - 1} \underbrace{C_n^{(1)}}_{\equiv C_n} \xrightarrow{\gamma \ll 1} (n+1) C_n^{(1)} \quad (42)$$

Plugging Eq. (42) into Eq. (41) we obtain Eq. (40). Comparing Eq. (40) with Eq. (39a) one can see that in the BFKL cascade

$$S_{d+2d}(Y) = S_{d+d}^2(Y) \quad (43)$$

Using Eq. (10), Eq. (8) and Eq. (42) we can calculate S_{d+2d} as follows

$$\begin{aligned} S_{d+2d}(Y) &= e^{-\tilde{Y}} \sum_{j=0}^{\infty} \frac{e^{\gamma n j} \tilde{Y}^j}{j!} \frac{e^{\gamma(n+1)} - 1}{e^\gamma - 1} (-\gamma N_j)^n n! \\ &= \frac{1}{\gamma} e^{-\tilde{Y}} \sum_{j=0}^{\infty} \frac{\tilde{Y}^j}{j!} \left\{ e^\gamma \frac{1}{\gamma e^{\gamma N_j}} \exp\left(\frac{1}{\gamma e^{\gamma N_j}}\right) \Gamma\left(0, \frac{1}{\gamma e^{\gamma N_j}}\right) - \frac{1}{\gamma N_j} \exp\left(\frac{1}{\gamma N_j}\right) \Gamma\left(0, \frac{1}{\gamma N_j}\right) \right\} \\ &\xrightarrow{\tilde{Y} \gg 1} e^{-\tilde{\Delta}_1 Y} \end{aligned} \quad (44)$$

where $\tilde{Y} \equiv \frac{\Delta}{\gamma} Y$.

Therefore, one can see that in the UTM Eq. (43) does not work. However, it turns out that we can get a simple formula for the Borel image of the scattering amplitude. Indeed, as we have seen in Eq. (13), for $S(Y)$ we can write:

$$S_{d+d}(\tilde{Y}) = e^{-\tilde{Y}} \sum_{j=0}^{\infty} \frac{\tilde{Y}^j}{j!} \int_0^{\infty} d\tau e^{-\tau} b_{d+d}^{(0)}(\tau, N_j) \quad \text{with} \quad N_j = \gamma e^{\gamma j} \quad (45)$$

In the region of small γ one can see from Eq. (42) that

$$S_{d+2d}(\tilde{Y}) = e^{-\tilde{Y}} \sum_{j=0}^{\infty} \frac{\tilde{Y}^j}{j!} \int_0^{\infty} d\tau e^{-\tau} b_{d+2d}^{(0)}(\tau, N_j) \quad \text{with} \quad b_{d+2d}^{(0)}(\tau, N_j) = \frac{d(\tau N_j b_{d+d}^{(0)}(\tau, N_j))}{d(\tau N_j)} \quad (46)$$

Using $b_{d+d}^{(0)}(\tau, N_j) = 1/(1 + \tau N_j)$ one can see that Eq. (40) for $b_{d+d}^{(0)}(\tau, N_j)$ takes a form:

$$b_{d+d}^{(0)}(\tau, N_{j+1}) - b_{d+d}^{(0)}(\tau, N_j) = \left(b_{d+d}^{(0)}(\tau, N_j)\right)^2 - b_{d+d}^{(0)}(\tau, N_j) \quad (47)$$

Therefore, for the Borel images equation has the same form as Eq. (40) if we replace $\frac{dS}{dY}$ by $b_{d+d}^{(0)}(\tau, N_{j+1}) - b_{d+d}^{(0)}(\tau, N_j)$ and N_0 by $1 - b_{d+d}^{(0)}$.

2. Single diffraction

In Ref.[78] it is shown that the equation for the cross section of the diffraction dissociation for the BFKL cascade can be written in the form:

$$\frac{d}{d\Delta Y} S_{d+d}^D(Y) = (S_{d+d}^D(Y))^2 - S_{d+d}^D(Y) \quad \text{where} \quad S^D = 1 - 2N_0 + \sigma_{sd} \quad (48)$$

In the UTM it takes the following form:

$$\frac{d}{d\Delta Y} S_{d+d}^D(Y) = (S_{d+2d}^D(Y)) - S_{d+d}^D(Y) \quad \text{where} \quad S^D = 1 - 2N_0 + \sigma_{sd} \quad (49)$$

with the same reasoning as in Eq. (41). For Borel images it translates to the equation:

$$b_{d+d}^{(D)}(\tau, N_{j+1}) - b_{d+d}^{(D)}(\tau, N_j) = b_{d+2d}^{(D)}(\tau, N_j) - b_{d+d}^{(D)}(\tau, N_j) = \left(b_{d+d}^{(D)}(\tau, N_j)\right)^2 - b_{d+d}^{(D)}(\tau, N_j) \quad (50)$$

In the region of small γ this equation can be rewritten in the form of Eq. (41), viz.:

$$b_{d+d}^{(sd)}(\tau, N_{j+1}) - b_{d+d}^{(sd)}(\tau, N_j) = b_{d+d}^{(sd)}(\tau, N_j) + \left(b_{d+d}^{(sd)}(\tau, N_j)\right)^2 - 4b_{d+d}^{(0)}(\tau, N_j) b_{d+d}^{(sd)}(\tau, N_j) + 2\left(b_{d+d}^{(sd)}(\tau, N_j)\right)^2 \quad (51)$$

As have been discussed the AGK cutting rules give

$$b_{d+d}^{(sd)}(\tau, N_j) = \frac{2(\tau\gamma N_j)^2}{(1 + \tau\gamma N_j)(1 + 2\tau\gamma N_j)} \quad (52)$$

We obtain Eq. (51) taking into account that

$$\begin{aligned} b_{d+2d}^{(sd)}(\tau, N_j) &= \frac{d}{d(\tau\gamma N_j)} \left(\tau\gamma N_j \underbrace{\left(\frac{2(\tau\gamma N_j)^2}{(1 + \tau\gamma N_j)(1 + 2\tau\gamma N_j)} \right)}_{b_{d+d}^{(sd)}(\tau, N_j)} \right) \\ &= 2b_{d+d}^{(sd)}(\tau, N_j) - 2\left(b_{d+d}^{(0)}(\tau, N_j)\right)^2 + \left(\frac{2\tau N_j}{1 + 2\tau\gamma N_j} \right)^2 \end{aligned} \quad (53)$$

3. σ_1

The equation for σ_1 takes the following form in the UTM:

$$\frac{d}{d\Delta Y}\sigma_1^{d+d}(Y) = \sigma_1^{d+2d}(Y) - \sigma_1^{d+d}(Y) \quad (54)$$

This equation can be rewritten for the Borel images as follows:

$$b_{d+d}^{(1)}(\tau, N_{j+1}) - b_{d+d}^{(1)}(\tau, N_j) = b_{d+d}^{(1)}(\tau, N_j) + 2b_{d+d}^{(1)}(\tau, N_j) b_{d+d}^{(sd)}(\tau, N_j) - 4b_{d+d}^{(0)}(\tau, N_j) b_{d+d}^{(1)}(\tau, N_j) \quad (55)$$

Using the AGK prediction for σ_1

$$b_{d+d}^{(1)}(\tau, N_j) = \frac{2\tau\gamma N_j}{(1 + 2\tau\gamma N_j)^2} \quad (56)$$

we obtain

$$b_{d+2d}^{(1)}(\tau, N_j) = \frac{d}{d(\tau\gamma N_j)} \left((\tau\gamma N_j) \underbrace{\left(\frac{2(\tau\gamma N_j)^2}{(1 + 2\tau\gamma N_j)^2} \right)}_{b_{d+d}^{(1)}(\tau, N_j)} \right) = 2b_{d+d}^{(1)}(\tau, N_j) - \frac{4(\tau\gamma N_j)^2}{(1 + 2\tau\gamma N_j)^3} \quad (57)$$

Plugging Eq. (57), Eq. (56) and Eq. (52) into Eq. (55) we see that this equation is correct.

4. σ_n

The equation for σ_n has the same general form as Eq. (54), viz.:

$$\frac{d}{d\Delta Y}\sigma_n^{d+d}(Y) = \sigma_n^{d+2d}(Y) - \sigma_n^{d+d}(Y) \quad (58)$$

Using that from AGK cutting rules the Borel image of σ_n^{d+d} (see Eq. (33)) is equal to

$$b_{d+d}^{(n)}(\tau, N_j) = \frac{(2\tau\gamma N_j)^n}{(1 + 2\tau\gamma N_j)^{n+1}} \quad (59)$$

and the Borel image of σ_n^{d+2d} can be written as follows

$$b_{d+2d}^{(n)}(\tau, N_j) = \frac{d}{dN_j} \left(N_j b_{d+d}^{(n)}(\tau, N_j) \right) \quad (60)$$

we obtain the following equation for $b_{d+d}^{(n)}(\tau, N_j)$

$$b_{d+d}^{(n)}(\tau, N_{j+1}) - b_{d+d}^{(n)}(\tau, N_j) = \quad (61)$$

$$b_{d+d}^{(n)}(\tau, N_j) + 2b_{d+d}^{(n)}(\tau, N_j) b_{d+d}^{(sd)}(\tau, N_j) + \sum_{k=1}^{n-1} b_{d+d}^{(n-k)}(\tau, N_j) b_{d+d}^{(k)}(\tau, N_j) - 4b_{d+d}^{(0)}(\tau, N_j) b_{d+d}^{(n)}(\tau, N_j)$$

In conclusion we see that the general equation in the UTM cascade has the form of Eq. (58) with $\sigma_0^{d+d} \equiv \sigma_{sd}$. These equation are equivalent to the AGK cutting rules and have natural form with clear physics meaning. In the case of the BFKL cascade these equation can be reduced to Eq. (39a) - Eq. (39e) that are shown in Fig. 5. In the region of small γ which models QCD approach, we can write the similar equations but for the Borel images of corresponding cross sections: see Eq. (47), Eq. (51), Eq. (55) and Eq. (61). These equation has the same form as Eq. (39a) - Eq. (39e) and can be written from them by replacing $\frac{d}{d\Delta Y}\sigma_n \rightarrow b_{d+d}^{(n)}(\tau, N_{j+1}) - b_{d+d}^{(n)}(\tau, N_j)$ and $\sigma_n \rightarrow b_{d+d}^{(n)}(\tau, N_j)$.

All equations for the BFKL cascade can be derived from the equation

$$\frac{d}{d\Delta Y} \underbrace{S_{in}(Y)}_{\text{select fixed multiplicity terms}} = \underbrace{(S_{in}(Y))^2 - S_{in}(Y)}_{\text{select fixed multiplicity terms}} \quad \text{where } S_{in} = 1 - 2N_0 + \sigma_{sd} + \sum_{n=1} \sigma_n \quad (62)$$

while for the UTM cascade Eq. (62) takes the form:

$$\underbrace{b_{in}(\tau, N_{j+1}) - b_{in}(\tau, N_j)}_{\text{select fixed multiplicity terms}} = \underbrace{(b_{in}(\tau, N_j))^2 - b_{in}(\tau, N_j)}_{\text{select fixed multiplicity terms}} \quad \text{where } b_{in} = 1 - 2b^{(0)} + b^{(sd)} + \sum_{n=1} b^{(n)} \quad (63)$$

V. ENTROPY OF PRODUCED PARTICLES

A. Continuous approximation

Here we will focus on the entropy of produced particles in the regime of large rapidities but $\gamma N(Y) \gg 1$ in the continuous approximation from Eq. (23),

$$\sigma_n = \frac{1}{\gamma N} K_0 \left(2\sqrt{\frac{n+1}{2\gamma N}} \right) \quad (64)$$

which is the probability to find n particles in the final state. In fact σ_n/σ_{in} , should be convoluted with $\mathcal{P}_n^{\text{Pom}}$ (see Eq. (28)), but at high energies, the latter can be approximated by a δ -function which plays no role in computation of the entropy.

The von Neumann entropy of the produced particles is:

$$S_E = - \sum_n \ln[\sigma_n/\sigma_{in}] \frac{\sigma_n}{\sigma_{in}} \quad (65)$$

Substituting Eq. (64) into Eq. (65) and switching from summation over n to integration over $\eta = 2\sqrt{\frac{n+1}{2\gamma N}}$, we obtain

$$S_E = \ln(2\gamma N) - \int_0^\infty \eta d\eta \ln[K_0(\eta)] K_0(\eta) \quad (66)$$

The integral over η equals -1.5 which does not depend on Y . Therefore, at large Y ,

$$S_E^{BFKL} = \ln[N_{BFKL}(Y)] + 1.5 \xrightarrow{Y \gg 1} \Delta Y; \quad N_{BFKL} = 2\gamma N(Y) \quad (67)$$

The result for the entropy coincides with the result of Ref.[55] but is quite different from Eq. (1). It is important to mention that Eq. (67) is different from (see Fig. 6)

$$S_E^{UTM} = \ln N_{UTM}; \quad N_{UTM} = \sum_n n P_n^{UTM} \quad (68)$$

It should be emphasize that Eq. (66) has a general origin: it stems from the KNO scaling behaviour[84] of the multiplicity distribution[16]. Indeed, if σ_n/σ_{in} has KNO behavior, viz.:

$$\frac{\sigma_n}{\sigma_{in}} = \frac{1}{\bar{n}} \Psi \left(\frac{n}{\bar{n}} \right) \quad (69)$$

where \bar{n} is a mean multiplicity, one can see that the entropy

$$S_E = \sum_n \ln \left(\frac{1}{\bar{n}} \Psi \left(\frac{n}{\bar{n}} \right) \right) \frac{1}{\bar{n}} \Psi \left(\frac{n}{\bar{n}} \right) = \ln \bar{n} + \sum \ln \left(\Psi \left(\frac{n}{\bar{n}} \right) \right) \frac{1}{\bar{n}} \Psi \left(\frac{n}{\bar{n}} \right) = \ln \bar{n} + \int d\zeta \ln(\Psi(\zeta)) \Psi(\zeta) \quad (70)$$

where $\zeta = n/\bar{n}$. The integral over ζ leads to the contribution which does not depend on Y , while $\ln \bar{n} = \Delta Y$.

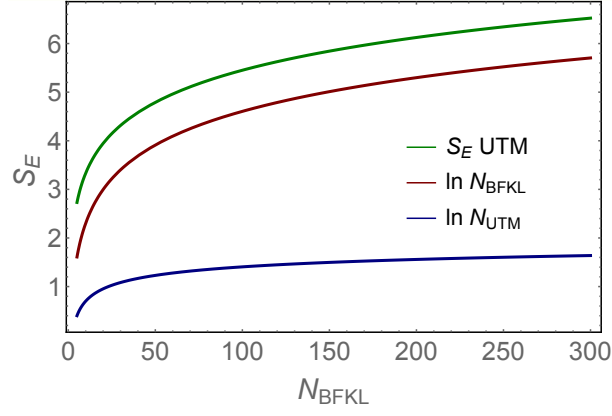


FIG. 6: Entropy comparison. S_E computed from the exact multiplicity distribution (66) in UTM versus $\ln[N_{UTM}/N_{BFKL}]$. $S_E^{BFKL} = \ln N_{BFKL}$, where N_{BFKL} is the mean multiplicity of produced dipoles in DIS. N_{UTM} is the mean multiplicity of dipoles in the initial state. $\Delta = 0.2$ and $\gamma = 0.025$.

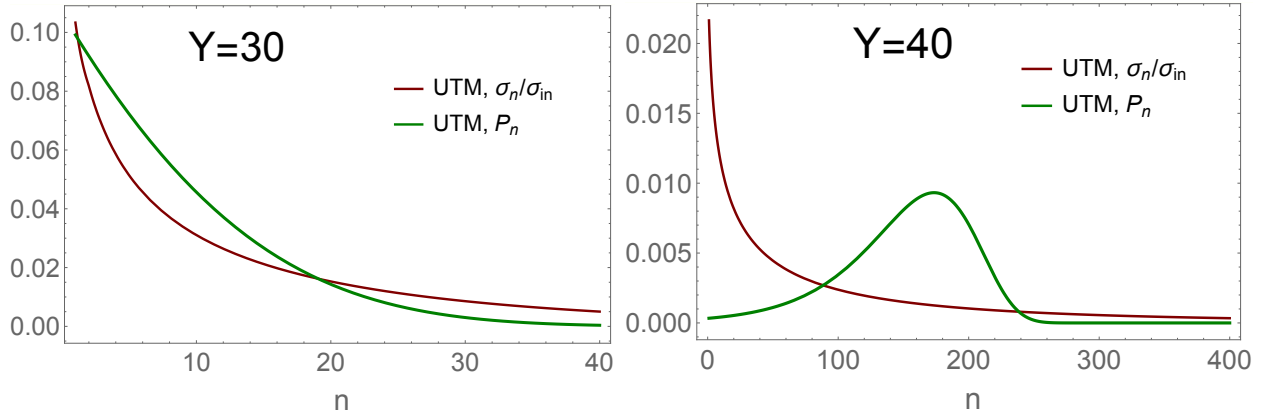


FIG. 7: σ_n/σ_{in} from Eq. (22) and $P_n = P_n^{UTM}$ for the parton cascade (see Ref.[16]) versus n at different Y . $\Delta = 0.2$ and $\gamma = 0.025$.

What is striking that while the entropy (65) $\sim \ln N_{BFKL}$, which is the result one would obtain for the BFKL cascade in DIS, the underlying multiplicity distributions for the particle production and for the parton cascade are quite different as illustrated in Fig. 7. Another explanation is that despite the same entropy of the produced particles (see Eq. (70)) and the entropy of the parton in the wave functions [16] the shape of distribution of the produced particles is quite different from P_n .

In Fig. 8 we plot the mean multiplicities for the initial and final states in the UTM. One can see that at large Y the much larger number of dipoles has been produced that it has the initial wave function.

B. Arbitrary Y

As has been discussed at large Y we can use Eq. (36) for σ_n/σ_{in} . This equation leads to the expression for the entropy of the same form as Eq. (66) but the integral over η has a more complex form being a function of \tilde{Y} . It is equal to

$$I(\tilde{Y}) = \frac{\int d\eta (2\sqrt{\eta} + \Delta\gamma Y\eta) \exp(-2\sqrt{\eta} - \Delta\gamma Y\eta)}{\int d\eta \exp(-2\sqrt{\eta} - \Delta\gamma Y\eta)} \rightarrow \begin{cases} 2 & \text{for } \Delta\gamma Y \ll 1; \\ 1 & \text{for } \Delta\gamma Y \gg 1; \end{cases} \quad (71)$$

Therefore, we can conclude that at large Y the entropy of produced dipoles is given by Eq. (67): $S_E = \Delta Y$. It should be noted that the same entropy was computed in the zero dimension model at $\tau = 0$ in Fig. 1 [55]. Hence,

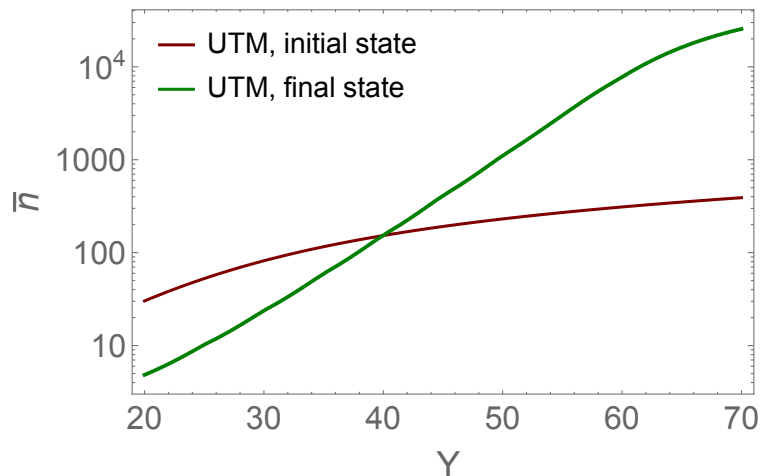


FIG. 8: The mean multiplicities in the UTM versus Y . $\Delta = 0.2$ and $\gamma = 0.025$.

in spite of the mess of interactions it turns out that the entropy of the parton cascade is not changed during its propagation from $\tau = 0$ to $\tau = \infty$.

VI. CONCLUSIONS

In this paper we found the multiplicity distribution of the produced dipoles in the final state for dipole-dipole scattering. This distribution show the great difference from the distributions of the parton in the wave function of the projectile. However, in spite of this difference the entropy of the produced dipoles turns out to be the same as the entropy of the dipoles in the wave function. This fact is not surprising since we have discussed in the paper that in the parton approach only dipoles in the hadron wave function can be produced at $t = +\infty$ and measured by the detectors. We also confirm the result of Ref.[55] that this entropy is equal to $S_E = \ln(xG(x))$, where we denote by xG the mean multiplicity of the dipoles in the deep inelastic scattering. This result contradicts the CGC-Black Hole correspondence , that has been suggested in Ref.[70].

Our results are based on AGK cutting rules but we derived the evolution equations for the partial cross sections σ_n which have the clear physics and reproduce the same results as the AGK cutting rules.

It should be stressed that we are able to consider in the zero dimension models not only DIS but the hadron-hadron scattering. The above result can be reformulated as the statement that the average multiplicity of produced dipoles coincides with mean multiplicity of the DIS for hadron-hadron collisions.

Second, we demonstrated a different mechanism for high energy multiparticle generation process ,which naturally arises in the zero dimension models from summing large Pomeron loops, and in which we do not need to produce a classical state with maximal entropy to satisfy t and s channel unitarity. We believe that this mechanism will work in QCD.

Acknowledgements

We thank our colleagues at Tel Aviv university for discussions. Our special thanks goes to Alex Kovner and Michael Lublinsky for the encouraging skepticism about AGK cutting rules which results in the appearance of section IV in the paper. This research was funded by Binational Science Foundation grant 2021789.

Appendix A: Distribution of the produced gluons in the BFKL Pomeron

Here we wish to stress that this follows from the general structure of the BFKL Pomeron in QCD[81]. Indeed, the BFKL equation has the general form in momentum representation:

$$\frac{\partial \phi_n(Y, k)}{\partial Y} = \int d^2 k' K(k, k') \phi_{n-1}(Y, k') \quad (\text{A1})$$

where ϕ_n is the cross section of n produced gluons and $K(k, k')$ is the kernel (see Ref.[81] for details). The eigenfunction of this equation are $(k^2)^\gamma$ and the general solution is the sum over these eigenfunctions

$$\phi_n(Y, k) = \sum_{\gamma} C(Y, n) (k^2)^\gamma \quad (\text{A2})$$

with the following equation for coefficients $C(Y, n)$:

$$\frac{\partial C(Y, n)}{\partial Y} = \chi(\gamma) C(Y, n-1) \quad (\text{A3})$$

where χ is the image of the BFKL kernel. One can check that the solution to Eq. (A3) takes the form:

$$C(Y, n) = \frac{(\chi(\gamma) Y)^n}{n!} \quad (\text{A4})$$

leading to

$$\phi_n(Y, k) = \int \frac{d\gamma}{2\pi i} \frac{(\chi(\gamma) Y)^n}{n!} (k^2)^\gamma \quad (\text{A5})$$

The cross section is equal to

$$\sigma_{tot} = \sum_{n=0}^{\infty} \phi_n(Y, k) = \int \frac{d\gamma}{2\pi i} e^{\chi(\gamma) Y} (k^2)^\gamma \quad (\text{A6})$$

while the probability to find n gluons in the final state is equal to

$$P_n = \frac{\phi_n(Y, k)}{\sigma_{tot}} = \frac{\int \frac{d\gamma}{2\pi i} \frac{(\chi(\gamma) Y)^n}{n!} (k^2)^\gamma}{\int \frac{d\gamma}{2\pi i} e^{\chi(\gamma) Y} (k^2)^\gamma} \quad (\text{A7})$$

At high energies the main contribution in Eq. (A7) can be estimated using the method of steepest descent with $\gamma_{SP} = \frac{1}{2}$. Bearing this in mind we see that Eq. (A7) give the Poisson distribution.

Appendix B: The Pomeron calculus of the UTM

In this appendix we wish to review what we know about the Pomeron calculus in zero dimension models and, particularly in the UTM. We have to admit that the majority of features of this calculus have been known for long time (see Refs.[1–10, 12–17]) but it turns out that a substantial part of these properties was preserved in my memory and I am sorry for not finding a proper references.

In our paper[15] we showed that the UTM model can be viewed as the Pomeron calculus with the following Hamiltonian:

$$\mathcal{H}_{\text{UTM}} = -\bar{\mathcal{P}} \mathcal{P} \quad (\text{B1})$$

where \mathcal{P} and $\bar{\mathcal{P}}$ are Pomeron operators, generates the rich Pomeron calculus. In Eq. (B2) we introduce $\tilde{Y} = \frac{\Delta}{\gamma} Y$. In the notations of this paper the Pomeron Hamiltonian is shown in Eq. (5) and it has a form:

$$\mathcal{H}_{\text{UTM}} = -t \left(1 - e^{\gamma(1-t)\frac{\partial}{\partial t}} \right) = \underbrace{\gamma t \frac{\partial}{\partial t}}_{\mathcal{H}_0} + t \underbrace{\left(e^{\gamma(1-t)\frac{\partial}{\partial t}} - 1 - \gamma \frac{\partial}{\partial t} \right)}_{\mathcal{H}_I} \quad (\text{B2})$$

where $u = 1 - t$ (see Ref.[?] for details). The choice of \mathcal{H}_0 is arbitrary and we did it based on the interpretation of the zero dimension models as the QCD with fixed dipole size. We have discussed this interpretation in the introduction (see Eq. (1)). This calculus have all vertices for $n\mathcal{P} \rightarrow m\mathcal{P}$ (V_m^n) interactions, in spite the evolution equation for P_n has only two vertices due to decay of one dipole to two (see Eq. (4)). It also gives the first and the only example of solvable simple Pomeron calculus with the infinite number of vertices. Expanding \mathcal{H}_I with respect to small γ one can see that in the order of γ we have the triple Pomeron vertex $\mathcal{P} \rightarrow 2\mathcal{P}$ (V_2^1) which is equal to $-\gamma$. In the order of γ^2 \mathcal{H}_I generates the correction to $V_1^1 = -\frac{1}{2}\gamma^2(\mathcal{P} \rightarrow \mathcal{P})$ and vertices $2\mathcal{P} \rightarrow \mathcal{P}$, $2\mathcal{P} \rightarrow 2\mathcal{P}$ and $2\mathcal{P} \rightarrow 3\mathcal{P}$. They are equal to $V_1^2 = \frac{1}{2}\gamma^2$, $V_2^2 = -\gamma^2$ and $V_3^2 = \frac{1}{2}\gamma^2$ (see Fig. 9).

1. The first Pomeron diagrams

The main features of the Pomeron calculus in the UTM can be seen just from the first diagrams (see Fig. 9). We will calculate them in ω representation, which is defined as

$$Z(u = 1 - tY) = \int_{\epsilon - i\infty}^{\epsilon + i\infty} \frac{d\omega}{2\pi i} e^{\omega \tilde{Y}} z(t, \omega) \quad (\text{B3})$$

Eq. (5) in this representation has the following form:

$$\mathcal{H}_{\text{UTM}} z(t, \omega) = (\mathcal{H}_0 + \mathcal{H}_I) z(t, \omega) = \omega z(t, \omega) \quad (\text{B4})$$

The first diagram of Fig. 9-a is the exchange of the 'bare' Pomeron, which gives the contribution

$$z(t = \gamma, \omega; \text{Fig. 9-a}) = \frac{\gamma}{\omega - \Delta} \quad \text{with} \quad \Delta = \gamma \quad (\text{B5})$$

where Δ is the intercept of the 'bare' Pomeron.

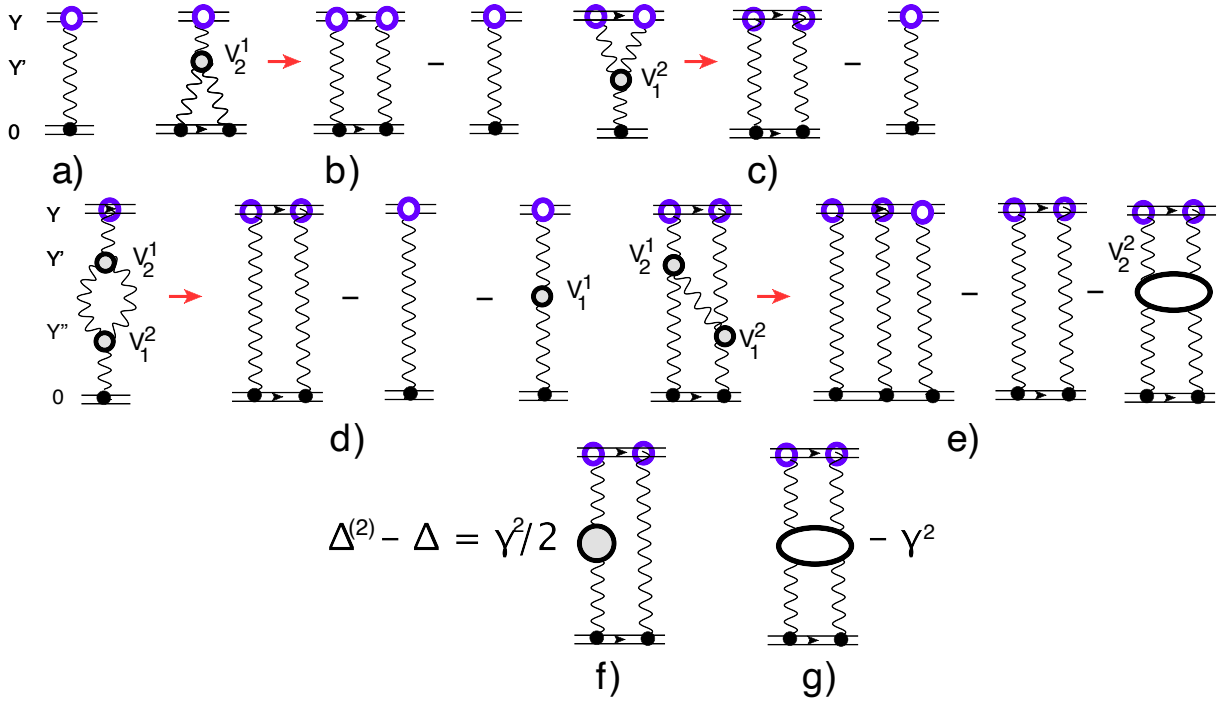


FIG. 9: The first Pomeron diagrams for $Z(u, Y)$. Fig. 9-a: the exchange of the Pomeron. Fig. 9-b and Fig. 9-c: the first semi-enhanced diagrams. Fig. 9-d: the diagrams for the Pomeron Green's function. Fig. 9-e the first diagrams for the two Pomeron Green's function. The black circle is the vertex of interaction of the Pomeron with the target, which is equal to $\gamma \frac{d}{dt}$. The blue circle is the vertex of interaction with the projectile dipole: $-t$. V_n^m are vertices of the transitions $mP \rightarrow nP$. $V_2^1 = \gamma t^2 \frac{d}{dt}$, $V_1^2 = \frac{1}{2} \gamma^2 t \frac{d^2}{dt^2}$, $V_1^1 = -\frac{1}{2} \gamma^2 t \frac{d}{dt}$, and V_2^2 is vertex for $2P \rightarrow 2P$ interaction, which is equal to $\frac{1}{2} \gamma^2 t^2 \frac{d^2}{dt^2}$.

The contribution of the diagram of Fig. 9-b takes the form

$$z(t = \gamma, \omega; \text{Fig. 9-b}) = -\frac{V_2^1 \gamma^2}{(\omega - \Delta)(\omega - 2\Delta)} = -\frac{V_2^1 \gamma^2}{\Delta} \left(\underbrace{\frac{1}{\omega - 2\Delta}}_{2P} - \underbrace{\frac{1}{\omega - \Delta}}_P \right) = -\frac{\gamma^2}{\omega - 2\Delta} + \frac{\gamma^2}{\omega - \Delta} \quad (\text{B6})$$

From Eq. (B6) one can see that the semi-enhanced diagram of Fig. 9-b give the new contribution, which is the exchange of two 'bare' Pomerons and the corrections to the vertex of the 'bare' Pomeron interaction with the target (see Fig. 9-a), which becomes $\gamma + \gamma^2$.

The diagram of Fig. 9- gives the same contribution. Indeed,

$$z(t = \gamma, \omega; Fig. 9 - c) = -\frac{2V_1^2\gamma}{(\omega - \Delta)(\omega - 2\Delta)} = -\frac{2V_1^2\gamma}{\Delta} \left(\underbrace{\frac{1}{\omega - 2\Delta}}_{2P} - \underbrace{\frac{1}{\omega - \Delta}}_P \right) = -\frac{\gamma^2}{\omega - 2\Delta} + \frac{\gamma^2}{\omega - \Delta} \quad (B7)$$

For V_1^2 we use $\frac{1}{2}\gamma\frac{d^2}{d\omega^2}$ as has been discussed above. It is instructive to note that in the BFKL cascade we do not have the diagram of Fig. 9-c and, therefore, the contribution of the two 'bare' Pomeron exchange is in two times less than in the UTM. This feature we can see directly from Eq. (13).

Now we calculate the first enhanced diagram of Fig. 9-d, whose contribution is equal to

$$\begin{aligned} z(t = \gamma, \omega; Fig. 9 - d) &= -\frac{V_2^1 2V_1^2 \gamma}{(\omega - \Delta)(\omega - 2\Delta)(\omega - \Delta)} = -\frac{V_2^1 2V_1^2 \gamma}{(\omega - \Delta)\Delta} \left(\frac{1}{\omega - 2\Delta} - \frac{1}{\omega - \Delta} \right) \\ &= -\frac{V_2^1 2V_1^2 \gamma}{\Delta} \left(\frac{1}{\Delta} \left(\underbrace{\frac{1}{\omega - 2\Delta}}_{2P} - \underbrace{\frac{1}{\omega - \Delta}}_P \right) - \underbrace{\frac{1}{(\omega - \Delta)^2}}_{\text{intercept } P} \right) \\ &= -\gamma^2 \left(\frac{1}{\omega - 2\Delta} - \frac{1}{\omega - \Delta} \right) + \boxed{\gamma^2} \gamma \frac{1}{(\omega - \Delta)^2} \end{aligned} \quad (B8)$$

The four diagrams that we have calculated exhaust the contribution of the order of γ^2 to the Green's function of the Pomeron. Collecting terms proportional to $1/(\omega - \Delta)$ we have the following contributions:

$$G_P(\omega) = \left(\gamma + \frac{3}{2}\gamma^2 \right) \frac{1}{\omega - \Delta} - \gamma \frac{\frac{1}{2}\gamma^2}{(\omega - \Delta)^2} \quad (B9)$$

Note that in the second term we took into account the contribution of V_1^1 in the order of γ^2 . It is easy to see that Eq. (B9) reproduce Eq. (13) if we expand both the Pomeron intercept and the impact factor to the order γ^2 .

Now we are going to evaluate the intercept of the two Pomeron Green's function. First contribution come from the exchange of two non-interacting Pomerons with a new intercept of the order of γ^2 (see Fig. 9-f): $\Delta^{(2)} = \Delta + \frac{1}{2}\gamma^2 = \gamma + \frac{1}{2}\gamma^2$, as we have found in Eq. (B9). The second contribution stems from Fig. 9-e. Indeed, this diagram is equal to

$$\begin{aligned} z(t = \gamma, \omega; Fig. 9 - e) &= 2\frac{V_2^1 2V_1^2 \gamma^2}{(\omega - 2\Delta)(\omega - 3\Delta)(\omega - 2\Delta)} = 2\frac{V_2^1 2V_1^2 \gamma^2}{(\omega - 2\Delta)\Delta} \left(\frac{1}{\omega - 3\Delta} - \frac{1}{\omega - 2\Delta} \right) \\ &= 2\frac{V_2^1 2V_1^2 \gamma^2}{\Delta} \left(\frac{1}{\Delta} \left(\underbrace{\frac{1}{\omega - 3\Delta}}_{3P} - \underbrace{\frac{1}{\omega - 2\Delta}}_{2P} \right) - \underbrace{\frac{1}{(\omega - 2\Delta)^2}}_{\text{intercept } 2P} \right) \\ &= \gamma^3 \left(\frac{1}{\omega - 3\Delta} - \frac{1}{\omega - 2\Delta} \right) - \boxed{2\gamma^2} \gamma^2 \frac{1}{(\omega - 2\Delta)^2} \end{aligned} \quad (B10)$$

In addition to Fig. 9-e and Fig. 9-f we need to calculate the diagram of Fig. 9-g, in which we take into account the vertex $V_2^2 = -\gamma^2$ for direct $2P \rightarrow 2P$ transition. Sum of all these contributions gives the intercept of G_{2P} $\Delta_2^{(2)} = 2\gamma + 2\gamma^2$ in accord with Eq. (13).

2. Summing enhanced diagrams

In this section we demonstrate that the intercepts for the Pomeron Green's function from Eq. (13) can be derived for the vertices $V_n^n = (e^\gamma - 1)^n$ (see Fig. 10). The simplest case is G_{2P} which is shown in Fig. 10-a. The bold wavy

lines denote the Pomeron with the intercept $\Delta_1 = e^\gamma - 1$. The sum of diagrams of Fig. 10-a has the following form

$$G_{2P}(\omega) = -\frac{1}{\omega - 2\Delta_1} - \frac{1}{\omega - 2\Delta_1} V_2^2 \frac{1}{\omega - 2\Delta_1} - \frac{1}{\omega - 2\Delta_1} V_2^2 \frac{1}{\omega - 2\Delta_1} V_2^2 \frac{1}{\omega - 2\Delta_1} - \dots = -\frac{1}{\omega - 2\Delta_1 - V_2^2} \quad (\text{B11})$$

Plugging $V_2^2 = (e^\gamma - 1)^2$ in Eq. (B11) we obtain

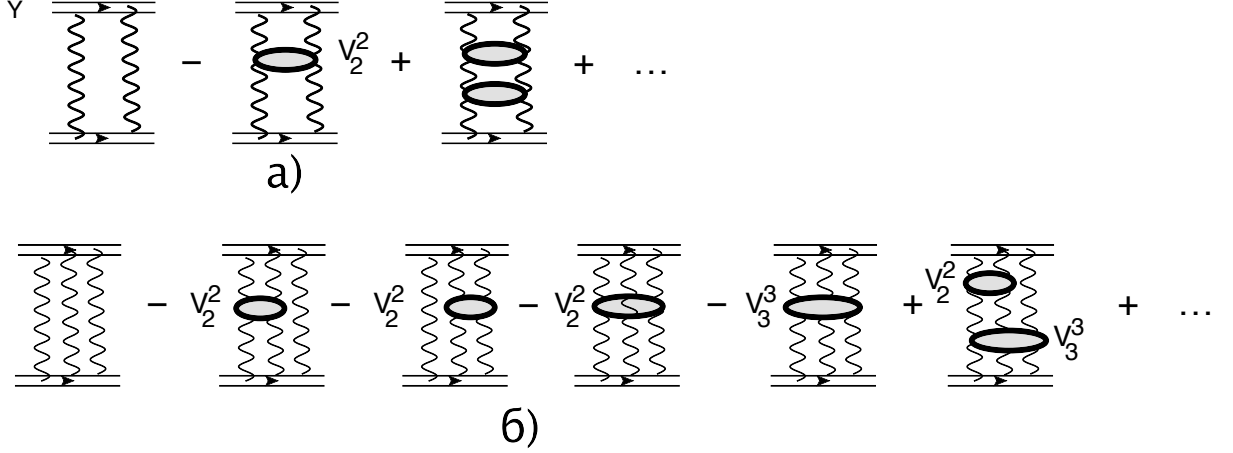


FIG. 10: The typical Pomeron diagrams in the UTM. Fig. 10-a: the diagrams for two Pomeron Green's function. Fig. 10-b: the diagrams for the three Pomeron Green's function. V_2^2 is vertex for $2P \rightarrow 2P$ interaction, while V_3^3 is vertex for $3P \rightarrow 3P$ interaction. The vertices V_n^n are equal to $(e^\gamma - 1)^n$.

$$G_{2P}(\omega) = -\frac{1}{\omega - 2(e^\gamma - 1) - (e^\gamma - 1)^2} = -\frac{1}{\omega - \Delta_2} = -\frac{1}{\omega - (e^{2\gamma} - 1)} \quad (\text{B12})$$

Hence Eq. (B12) reproduces the exchange of two Pomerons in Eq. (13).

For $G_{3P}(\omega)$ of Fig. 10-b we have

$$G_{3P}(\omega) = \frac{1}{\omega - 3\Delta_1} + \frac{1}{\omega - 3\Delta_1} (3V_2^2 + V_3^3) \frac{1}{\omega - 3\Delta_1} + \frac{1}{\omega - 3\Delta_1} (3V_2^2 + V_3^3) \frac{1}{\omega - 3\Delta_1} (3V_2^2 + V_3^3) \frac{1}{\omega - 3\Delta_1} + \dots = -\frac{1}{\omega - 3\Delta_1 - 3V_2^2 - V_3^3} \quad (\text{B13})$$

Taking into account that $V_2^2 = (e^\gamma - 1)^2$ and $V_3^3 = (e^\gamma - 1)^3$ we have

$$G_{3P}(\omega) = -\frac{1}{\omega - 3(e^\gamma - 1) - 3(e^\gamma - 1)^2 - (e^\gamma - 1)^3} = -\frac{1}{\omega - \Delta_2} = -\frac{1}{\omega - (e^{3\gamma} - 1)} \quad (\text{B14})$$

which reproduces the intercept of the third term in Eq. (13). It is easy to generalize the derivation to $G_{nP}(\omega)$.

Therefore, the scattering amplitude of Eq. (7) has simple and apparent meaning: each term is the Green's function for the exchange of n -Pomerons which is given by the factor $\exp(\Delta_n \tilde{Y})$ (see Fig. 10). Factors $C_n(\gamma) \Phi_n(e^{-\gamma}, \gamma)$ are the residues (impact factors) of the Green's function. Each term is intimately related to the inclusive production of one, two and so on particles[?], and, therefore, has a direct physics meaning. The series of Eq. (7) is a typical example of the asymptotic series, sum of which is the analytical function that has the same expansion. In our paper [17] we proposed the way of summing this asymptotic series.

3. Multiplicity distribution for the 'dressed' Pomeron

In section 3.2 we assumed that the 'dressed' Pomeron has the same Poisson distribution of the produced dipoles as the 'bare' Pomeron. Fig. 11 illustrates this point of view considering the first enhanced diagram for the 'dressed' Pomeron.

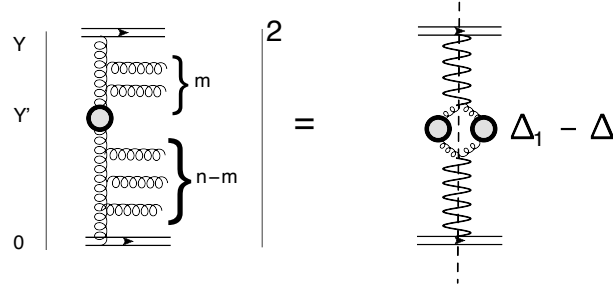


FIG. 11: The multiplicity distribution for the first enhanced diagram in the 'dressed' Pomeron. The wavy line denotes the cut Pomeron. Helix lines describe the partons. $\Delta_1 = e^\gamma - 1$ and $\Delta = \gamma$ is the intercept of the 'bare' Pomeron.

The σ_n for this diagram is equal to

$$\sigma_n = \int_0^Y dY' \gamma (\Delta_1 - \Delta) \sum_{m=1}^n \frac{(\Delta(Y-Y'))^m}{m!} e^{-\Delta(Y-Y')} \frac{(\Delta(Y-Y'))^{n-m}}{(n-m)!} e^{-\Delta Y'} = (\Delta_1 - \Delta) Y \frac{(\Delta Y)^n}{n!} e^{-\Delta Y} \quad (\text{B15})$$

Sum of all enhanced diagrams leads to

$$\frac{\sigma_n^{\mathcal{P}}}{\sigma_{in}^{\mathcal{P}}} = \frac{(\Delta Y)^n}{n!} e^{-\Delta Y} \quad (\text{B16})$$

Eq. (B16) is the Poisson distribution, the same as for the 'bare' Pomeron in Eq. (2).

* Electronic address: leving@tauex.tau.ac.il

- [1] D. Amati, L. Caneschi and R. Jengo, Nucl. Phys. B **101** (1975) 397.
- [2] V. Alessandrini, D. Amati and R. Jengo, Nucl. Phys. B **108** (1976) 425.
- [3] R. Jengo, Nucl. Phys. B **108** (1976) 447.
- [4] D. Amati, M. Le Bellac, G. Marchesini and M. Ciafaloni, Nucl. Phys. B **112** (1976) 107.
- [5] M. Ciafaloni, M. Le Bellac and G. C. Rossi, Nucl. Phys. B **130** (1977) 388.
- [6] M. Ciafaloni, Nucl. Phys. B **146** (1978) 427.
- [7] A. H. Mueller and G. P. Salam, Nucl. Phys. B **475**, 293 (1996), [hep-ph/9605302]; G. P. Salam, Nucl. Phys. B **461**, 512 (1996), [hep-ph]
- [8] P. Rembiesa and A. M. Stasto, Nucl. Phys. B **725** (2005) 251.
- [9] A. I. Shoshi and B. W. Xiao, Phys. Rev. D **73** (2006) 094014.
- [10] M. Kozlov and E. Levin, Nucl. Phys. A **779** (2006) 142.
- [11] S. Bondarenko, L. Motyka, A. H. Mueller, A. I. Shoshi and B. W. Xiao, Eur. Phys. J. C **50** (2007), 593-601, [arXiv:hep-ph/0609213 [hep-ph]].
- [12] J.-P. Blaizot, E. Iancu and D. N. Triantafyllopoulos, Nucl. Phys. A **784** (2007) 227.
- [13] N. Armesto, S. Bondarenko, J. G. Milhano and P. Quiroga, JHEP 0805 (2008) 103.
- [14] E. Levin and A. Prygarin, Eur. Phys. J. C **53** (2008) 385.
- [15] A. Kovner, E. Levin and M. Lublinsky, JHEP **08** (2016), 031.
- [16] A. Kovner, E. Levin and M. Lublinsky, JHEP **05**, 019 (2022) [arXiv:2201.01551 [hep-ph]].
- [17] A. Kovner, E. Levin and M. Lublinsky, JHEP **10** (2024), 127 [arXiv:2406.12691 [hep-ph]].
"High energy scattering in the Unitary Toy Model," [arXiv:2406.12691 [hep-ph]].
- [18] V. Andreev *et al.* [H1], Eur. Phys. J. C **81** (2021) no.3, 212 doi:10.1140/epjc/s10052-021-08896-1 [arXiv:2011.01812 [hep-ex]].
- [19] C. Adloff *et al.* [H1], "Multiplicity structure of the hadronic final state in diffractive deep inelastic scattering at HERA," Eur. Phys. J. C **5** (1998), 439-452 doi:10.1007/s100529800963 [arXiv:hep-ex/9804012 [hep-ex]].
- [20] C. Adloff *et al.* [H1], "Evolution of $e p$ fragmentation and multiplicity distributions in the Breit frame," Nucl. Phys. B **504** (1997), 3-23 doi:10.1016/S0550-3213(97)00585-3 [arXiv:hep-ex/9707005 [hep-ex]].
- [21] S. Chekanov *et al.* [ZEUS], "Energy dependence of the charged multiplicity in deep inelastic scattering at HERA," JHEP **06** (2008), 061 doi:10.1088/1126-6708/2008/06/061 [arXiv:0803.3878 [hep-ex]].
- [22] M. Aaboud *et al.* [ATLAS], Eur. Phys. J. C **76** (2016) no.9, 502 doi:10.1140/epjc/s10052-016-4335-y [arXiv:1606.01133 [hep-ex]].
- [23] G. Aad *et al.* [ATLAS], Phys. Lett. B **758** (2016), 67-88 doi:10.1016/j.physletb.2016.04.050 [arXiv:1602.01633 [hep-ex]].

- [24] G. Aad *et al.* [ATLAS], Eur. Phys. J. C **76** (2016) no.7, 403 doi:10.1140/epjc/s10052-016-4203-9 [arXiv:1603.02439 [hep-ex]].
- [25] G. Aad *et al.* [ATLAS], New J. Phys. **13** (2011), 053033 doi:10.1088/1367-2630/13/5/053033 [arXiv:1012.5104 [hep-ex]].
- [26] G. Aad *et al.* [ATLAS], Phys. Lett. B **688** (2010), 21-42 doi:10.1016/j.physletb.2010.03.064 [arXiv:1003.3124 [hep-ex]].
- [27] Y. Kulchitsky and P. Tsiarshka, Study of the KNO scaling in pp collisions at \sqrt{s} from 0.9 to 13 TeV using results of the ATLAS at the LHC, Eur. Phys. J. C **82** (2022) 462, arXiv: 2202.06697 [hep-ex].
- [28] A. M. Sirunyan *et al.* [CMS], Eur. Phys. J. C **78** (2018) no.9, 697 doi:10.1140/epjc/s10052-018-6144-y [arXiv:1806.11245 [hep-ex]].
- [29] V. Khachatryan *et al.* [CMS], Phys. Lett. B **751** (2015), 143-163 doi:10.1016/j.physletb.2015.10.004 [arXiv:1507.05915 [hep-ex]].
- [30] V. Khachatryan *et al.* [CMS], JHEP **01** (2011), 079 doi:10.1007/JHEP01(2011)079 [arXiv:1011.5531 [hep-ex]].
- [31] V. Khachatryan *et al.* [CMS], Phys. Rev. Lett. **105** (2010), 022002 doi:10.1103/PhysRevLett.105.022002 [arXiv:1005.3299 [hep-ex]].
- [32] V. Khachatryan *et al.* [CMS], JHEP **02** (2010), 041 doi:10.1007/JHEP02(2010)041 [arXiv:1002.0621 [hep-ex]].
- [33] S. Chatrchyan *et al.* [CMS and TOTEM], Eur. Phys. J. C **74** (2014) no.10, 3053 doi:10.1140/epjc/s10052-014-3053-6 [arXiv:1405.0722 [hep-ex]].
- [34] G. Antchev *et al.* [TOTEM], Eur. Phys. J. C **75** (2015) no.3, 126 doi:10.1140/epjc/s10052-015-3343-7 [arXiv:1411.4963 [hep-ex]].
- [35] K. Aamodt *et al.* [ALICE], Eur. Phys. J. C **68** (2010), 89-108 doi:10.1140/epjc/s10052-010-1339-x [arXiv:1004.3034 [hep-ex]].
- [36] K. Aamodt *et al.* [ALICE], Eur. Phys. J. C **68** (2010), 345-354 doi:10.1140/epjc/s10052-010-1350-2 [arXiv:1004.3514 [hep-ex]].
- [37] J. Adam *et al.* [ALICE], Phys. Lett. B **753** (2016), 319-329 doi:10.1016/j.physletb.2015.12.030 [arXiv:1509.08734 [nucl-ex]].
- [38] J. Adam *et al.* [ALICE], Eur. Phys. J. C **77** (2017) no.1, 33 doi:10.1140/epjc/s10052-016-4571-1 [arXiv:1509.07541 [nucl-ex]].
- [39] S. Acharya *et al.* [ALICE], Eur. Phys. J. C **77** (2017) no.12, 852 doi:10.1140/epjc/s10052-017-5412-6 [arXiv:1708.01435 [hep-ex]].
- [40] S. Acharya *et al.* [ALICE], Eur. Phys. J. C **79** (2019) no.10, 857 doi:10.1140/epjc/s10052-019-7350-y [arXiv:1905.07208 [nucl-ex]].
- [41] R. Aaij *et al.* [LHCb], Eur. Phys. J. C **74** (2014) no.5, 2888, [arXiv:1402.4430 [hep-ex]].
- [42] R. Aaij *et al.* [LHCb], Eur. Phys. J. C **72** (2012), 1947 doi:10.1140/epjc/s10052-012-1947-8 [arXiv:1112.4592 [hep-ex]].
- [43] EHS/NA22 Collaboration, Phase Space Dependence of the Multiplicity Distribution in π^+p and pp Collisions at 250-GeV/c, Z. Phys. C **37** (1988) 215.
- [44] UA1 Collaboration, A Study of the General Characteristics of $p\bar{p}$ Collisions at $\sqrt{s} = 0.2$ -TeV to 0.9-TeV, Nucl. Phys. B **335** (1990) 261.
- [45] UA5 Collaboration, An Investigation of Multiplicity Distributions in Different Pseudorapidity Intervals in anti-p p Reactions at a CMS Energy of 540-GeV, Phys. Lett. B **160** (1985) 193.
- [46] UA5 Collaboration, Charged Particle Multiplicity Distributions at 200-GeV and 900-GeV Center-Of-Mass Energy, Z. Phys. C **43** (1989) 357, ed. by R. Kotthaus and J. H. Kuhn.
- [47] T. Aaltonen *et al.* [CDF], Phys. Rev. D **79** (2009), 112005 [erratum: Phys. Rev. D **82** (2010), 119903] doi:10.1103/PhysRevD.79.112005 [arXiv:0904.1098 [hep-ex]].
- [48] T. Aaltonen *et al.* [CDF], Phys. Rev. D **79** (2009), 112005 [erratum: Phys. Rev. D **82** (2010), 119903] doi:10.1103/PhysRevD.79.112005 [arXiv:0904.1098 [hep-ex]].
- [49] CDF Collaboration, Pseudorapidity distributions of charged particles produced in $p\bar{p}$ interactions at $\sqrt{s}=630$ GeV and 1800 GeV. FERMILAB-PUB-89-201-E, p. 119 (1989), ed. by J. Tran Thanh Van
- [50] R. Schicker [ALICE], “Overview of ALICE results in pp , pA and AA collisions,” EPJ Web Conf. **138** (2017), 01021 doi:10.1051/epjconf/201713801021 [arXiv:1701.04810 [nucl-ex]].
- [51] K. Kutak, Phys. Lett. B **705** (2011), 217-221 [arXiv:1103.3654 [hep-ph]].
- [52] R. Peschanski, Phys. Rev. D **87** (2013) no.3, 034042 [arXiv:1211.6911 [hep-ph]].
- [53] A. Kovner and M. Lublinsky, Phys. Rev. D **92** (2015) no.3, 034016 [arXiv:1506.05394 [hep-ph]].
- [54] R. Peschanski and S. Seki, Phys. Lett. B **758** (2016), 89-92 [arXiv:1602.00720 [hep-th]].
- [55] D. E. Kharzeev and E. M. Levin, Phys. Rev. D **95** (2017) no.11, 114008 [arXiv:1702.03489 [hep-ph]].
- [56] O. Baker and D. Kharzeev, Phys. Rev. D **98** (2018) no.5, 054007 [arXiv:1712.04558 [hep-ph]].
- [57] J. Berges, S. Floerchinger and R. Venugopalan, JHEP **04** (2018), 145 [arXiv:1712.09362 [hep-th]].
- [58] Y. Hagiwara, Y. Hatta, B. W. Xiao and F. Yuan, Phys. Rev. D **97** (2018) no.9, 094029 [arXiv:1801.00087 [hep-ph]].
- [59] N. Armesto, F. Dominguez, A. Kovner, M. Lublinsky and V. Skokov, JHEP **05** (2019), 025 [arXiv:1901.08080 [hep-ph]].
- [60] E. Gotsman and E. Levin, Eur. Phys. J. C **79** (2019) no.5, 415 [arXiv:1902.07923 [hep-ph]].
- [61] E. Gotsman and E. Levin, Phys. Rev. D **100** (2019) no.3, 034013 [arXiv:1905.05167 [hep-ph]].
- [62] A. Kovner, M. Lublinsky and M. Serino, Phys. Lett. B **792** (2019), 4-15 [arXiv:1806.01089 [hep-ph]].
- [63] D. Neill and W. J. Waalewijn, Phys. Rev. Lett. **123** (2019) no.14, 142001 [arXiv:1811.01021 [hep-ph]].
- [64] Y. Liu and I. Zahed, Phys. Rev. D **100** (2019) no.4, 046005 [arXiv:1803.09157 [hep-ph]].
- [65] X. Feal, C. Pajares and R. Vazquez, Phys. Rev. C **99** (2019) no.1, 015205 [arXiv:1805.12444 [hep-ph]].
- [66] Z. Tu, D. E. Kharzeev and T. Ullrich, Phys. Rev. Lett. **124** (2020) no.6, 062001 [arXiv:1904.11974 [hep-ph]].
- [67] H. Duan, C. Akkaya, A. Kovner and V. V. Skokov, Phys. Rev. D **101** (2020) no.3, 036017 [arXiv:2001.01726 [hep-ph]].
- [68] C. Akkaya and A. Kovner, “On Entanglement Entropy of Maxwell fields in $3+1$ dimensions with a slab geometry,”

- [arXiv:2007.15970 [hep-th]].
- [69] M. Hentschinski, K. Kutak and R. Straka, Eur.Phys.J. **C 82** (2022) 12, 1147, [arXiv:2207.09430 [hep-ph]].
- [70] G. Dvali and R. Venugopalan, Phys. Rev. D **105**, no.5, 056026 (2022), [arXiv:2106.11989 [hep-th]].
- [71] G. Dvali, JHEP **03**, 126 (2021), [arXiv:2003.05546 [hep-th]].
- [72] G. Dvali, ‘*Classicalization Clearly: Quantum Transition into States of Maximal Memory Storage Capacity*,’ [arXiv:1804.06154 [hep-th]].
- [73] A. H. Mueller, Nucl. Phys. B **415** (1994) 373; Nucl. Phys. B **437** (1995) 107; A. H. Mueller and B. Patel, Nucl. Phys. B **425**, 471, 1994.
- [74] A. Kovner and M. Lublinsky, Nucl. Phys. A **767** 171 (2006).
- [75] V. A. Abramovsky, V. N. Gribov and O. V. Kancheli, Yad. Fiz. **18** (1973), 595, (Sov.J. Nucl.Phys. 18 (1974),308);
- [76] M. Abramowitz and I. Stegun, ‘*Handbook of Mathematical Functions with Formulas, Graphs, and Mathematical Tables*’, United States Department of Commerce, National Bureau of Standards,1964
- [77] Yuri V. Kovchegov and Eugene Levin, ‘*Quantum Chromodynamics at High Energies*’, Cambridge Monographs on Particle Physics, Nuclear Physics and Cosmology, Cambridge University Press, 2012 .
- [78] Y. V. Kovchegov and E. Levin, Nucl. Phys. B **577** (2000), 221-239 doi:10.1016/S0550-3213(00)00125-5 [arXiv:hep-ph/9911523 [hep-ph]].
- [79] Z. Chen and A. H. Mueller, Nucl. Phys. B **451** (1995), 579-604 doi:10.1016/0550-3213(95)00350-2
- [80] A. Kormilitzin, E. Levin and A. Prygarin, Nucl. Phys. A **813** (2008), 1-13 doi:10.1016/j.nuclphysa.2008.09.006 [arXiv:0807.3413 [hep-ph]].
- [81] V. S. Fadin, E. A. Kuraev and L. N. Lipatov, Phys. Lett. **B60**, 50 (1975); E. A. Kuraev, L. N. Lipatov and V. S. Fadin, Sov. Phys. JETP **45**, 199 (1977), [Zh. Eksp. Teor. Fiz.72,377(1977)]; I. I. Balitsky and L. N. Lipatov, Sov. J. Nucl. Phys. **28**, 822 (1978), [Yad. Fiz.28,1597(1978)].
- [82] E. Levin, Phys. Rev. D **49** (1994), 4469-4480.
- [83] L. Caneschi (ed.), Regge Theory of Low- p T Hadronic Interaction (North-Holland, Amsterdam, 1989)
- [84] A.M. Polyakov, Zh. Eksp. Teor. Fiz. **59**, 542 (1970); Z. Koba, H.B. Nielsen and P. Olesen, Nucl. Phys. **B40**, 317 (1972); Z. Koba, in Proc. of the 1973 CERN School of Physics, p. 171, CERN Yellow Report CERN-73-12 (1973).